

Photocatalysis

Tunable Isometric Donor-Acceptor Wurster-Type Covalent Organic Framework Photocathodes

Roman Guntermann⁺, David Helminger⁺, Laura Frey, Peter M. Zehetmaier, Christian Wangnick, Apeksha Singh, Tianhao Xue, Dana D. Medina,^{*} and Thomas Bein^{*}

Abstract: Covalent organic frameworks (COFs) offer remarkable versatility, combining ordered structures, high porosity, and tailorable functionalities in nanoscale reaction spaces. Herein, we report the synthesis of a series of isostructural, photoactive Wurster-type COFs achieved by manipulating the chemical and electronic nature of the Wurster aromatic amine building blocks. A series of donor-acceptor-donor (D-A-D) Wurster building block molecules was synthesized by incorporating heteroaromatic acceptors with varying strengths between triphenylamine donor groups. These tailored building blocks were integrated into a 2D COF scaffold, resulting in highly crystalline structures and similar morphologies across all COFs. Remarkably, this structural uniformity was also achieved in the synthesis of homogeneous and oriented thin films. Steady-state photoluminescence revealed a tunable red-shift in film emission exceeding 100 nm, demonstrating effective manipulation of their optical properties. Furthermore, photoelectrochemical (PEC) water splitting studies exhibited a doubled current density ($8.1 \mu\text{A cm}^{-2}$ at $0.2 V_{\text{RHE}}$) for the COF with the strongest acceptor unit. These findings highlight the potential of Wurster D-A-D COFs in photoelectrochemical water splitting devices and pave the way for further exploration of chemical functionality-reactivity-property relationships in this promising class of photoactive materials.

Introduction

The ability to precisely control and predesign materials properties is a highly desirable feature in materials science. Covalent organic frameworks (COFs), a class of crystalline porous polymers, stand out in this regard by virtue of their synthesis principles of reticular chemistry, offering an enormous scope for the design of functional materials.^[1] This aspect together with advantages such as high accessible surface areas and high stability have qualified COFs primarily for applications such as gas and energy storage,^[2] as well as optoelectronics^[3] and electrocatalysis.^[4] In recent years, their scope could be further expanded, for example in the realm of active photocatalysts for water splitting.^[5,6] To harvest and convert photons, it is often desirable to present the COF in the form of thin films. Considerable effort is being devoted to the design of suitable thin film characteristics to efficiently harvest light and to use photogenerated charge carriers in the COFs. Hence, various techniques such as solvothermal synthesis,^[6] electrophoretic deposition^[7] and solution-processing^[8] have been developed to optimize thin film features such as orientation and optical, electrical or chemical properties with a view on specific functionalities.

One promising approach for optical tuning is the use of isomeric structures to achieve predictable alteration of the optical properties.^[9] Exploring isomeric structures as a means for band gap engineering recently enabled us to fine-tune the COF band gap by controlling the blending ratio of isomeric building blocks embedded in the framework.^[10] While isomer blending enables fine-tuning of the band gap, larger changes of the band gap typically require varying the molecular and functional composition in the COF backbone, or modifying the stacking and crystallinity of the resulting frameworks.^[11] One elaborate process is the predesign of building blocks with desired functionalities or different extent of conjugation within monomers.^[12] Notably, the combination of donor-acceptor (D-A) moieties embedded in the COF can offer wide-ranging control over the band gap and band alignment of the COF.^[13,14] Moreover, the distinctive electronic nature of D-A systems can provide electron-hole separation ability attributed to strong intramolecular charge-transfer (CT) interactions in the COF that are tunable by employing different types of donor or acceptor groups.^[15]

We have recently reported Wurster-based COFs constructed from a Wurster precursor (*N,N,N',N'*-tetrakis(4-aminophenyl)-1,4-phenylenediamine) bearing two covalently-linked triphenyl amine donor moieties. This architec-

[*] R. Guntermann,⁺ D. Helminger,⁺ Dr. L. Frey, Dr. P. M. Zehetmaier, C. Wangnick, A. Singh, T. Xue, Dr. D. D. Medina, Prof. Dr. T. Bein
 Department of Chemistry and Center for Nanoscience (CeNS)
 Ludwig-Maximilians-Universität (LMU)
 Butenandtstraße 11 (E)
 81377 Munich, Germany
 E-mail: dana.medina@cup.lmu.de
 bein@lmu.de

[†] These authors contributed equally to this work.

© 2024 The Authors. Angewandte Chemie International Edition published by Wiley-VCH GmbH. This is an open access article under the terms of the Creative Commons Attribution Non-Commercial NoDerivs License, which permits use and distribution in any medium, provided the original work is properly cited, the use is non-commercial and no modifications or adaptations are made.

ture facilitates the stabilization of radical ions within the π -system. Subsequent chemical doping of these Wurster-COFs with iodine or F_4TCNQ resulted in strongly enhanced electrical conductivity of a COF bearing high concentrations of radicals.^[16] Furthermore, the synergy between the strong donor capability and the reversible redox system renders Wurster-type COFs as excellent platform for the oxygen reduction reaction (ORR), the oxygen evolution reaction (OER),^[17] or H_2O_2 generation.^[18] Extending this concept, the combination of the electron-rich Wurster-motif with benzothiadiazole acceptor units resulted in electrochromic COF films exhibiting a reversible dark-to-transparent switch.^[19] This initial example for a D-A combination in Wurster-type COFs demonstrates the enormous potential for various functionalities and applications by combining the strong Wurster donor motif with electron-deficient moieties.

Herein, we have isometrically altered the (aldehyde-functionalized) Wurster motif with a series of central aromatic electron-deficient units namely, phenyl (P), the isomeric pyrimidine (Pm) and pyridazine (Pz), and [1,2,5]thiadiazolo[3,4-c]pyridine (Tz), thus creating a set of novel COF building blocks according to known synthesis strategies.^[20–22] By installing these modified aldehyde-functionalized Wurster building blocks into 2D imine-linked COFs in combination with the original Wurster amine (W) node, four new, highly crystalline and isostructural COFs with unique electronic architectures were synthesized and fully characterized. Subsequently, the influence of the central A-moieties in the D-A-D-type building blocks on the optical properties of the respective COFs was studied. Moreover, we demonstrate the impact of the electron-withdrawing moieties on the optical features of solvothermally grown COF thin films and on their photoelectrochemical (PEC) water splitting efficiency. These studies enable a systematic understanding of structure-property relationships, enabling tailorable design of materials with desired functionalities for applications such as catalytic water oxidation. With this study, we establish the power and versatility of isometric substitution in D-A COF building blocks for the wide-ranging control of their physical properties, with a view on diverse optoelectronic functionalities.

Results and Discussion

Preparation of Aldehyde Chromophores

To create the new aldehyde-modified monomers for imine COFs, a synthesis procedure reported in the literature was utilized.^[21] This involved coupling diiodides or dibromides via the Suzuki reaction with the corresponding aldehyde-functionalized boronic acid. This process was carried out in the presence of a Pd(0) catalyst, resulting in the formation of X-BTPA tetraaldehyde monomers (Figures 1a, S1, and see section B in the Supporting Information). The acronym BTPA stands for bistriphenylamine. As central aromatic or heterocyclic aromatic groups, (X), phenyl (P), the isomeric pyrimidine (Pm) and pyridazine (Pz) and [1,2,5]thiadiazolo[3,4-c]pyridine (Tz) were chosen due to their distinct increasing electron-withdrawing character and for Pm, Pz and Tz due to their successful use in photocatalytic systems.^[14,23] Similar triphenylamine-based donor-acceptor dyes are known for their strong emission in their aggregated forms.^[20] These building blocks were first analyzed individually by optical spectroscopy to investigate the influence of different electron-withdrawing groups in the central core of the molecules. To avoid solvent effects on the intramolecular charge transfer (ICT) of the D-A-D monomers, resulting in shifts of the absorption and emission bands,^[20] the optical properties were measured for non-crystalline powders. However, it is possible that potential shifts may occur due to variations in monomer aggregation. Wurster amine, the later counterpart for the aldehyde monomers for the COF synthesis, has a photoluminescence (PL) emission maximum at the shortest wavelength at 453 nm and a more distinct and narrower band compared with the X-BTPA monomers (Figure 1b). The emission at higher photon energies is attributed to the shorter π -electron conjugation and the absence of a central electronically distinct acceptor (A) unit in the smaller molecule. In contrast to W, all D-A-D chromophores showed a strong absorption band between 300 and 600 nm in the UV/Vis spectral range, attributed to the intramolecular charge-transfer (ICT) transition.^[20,24] The strong electron-withdraw-

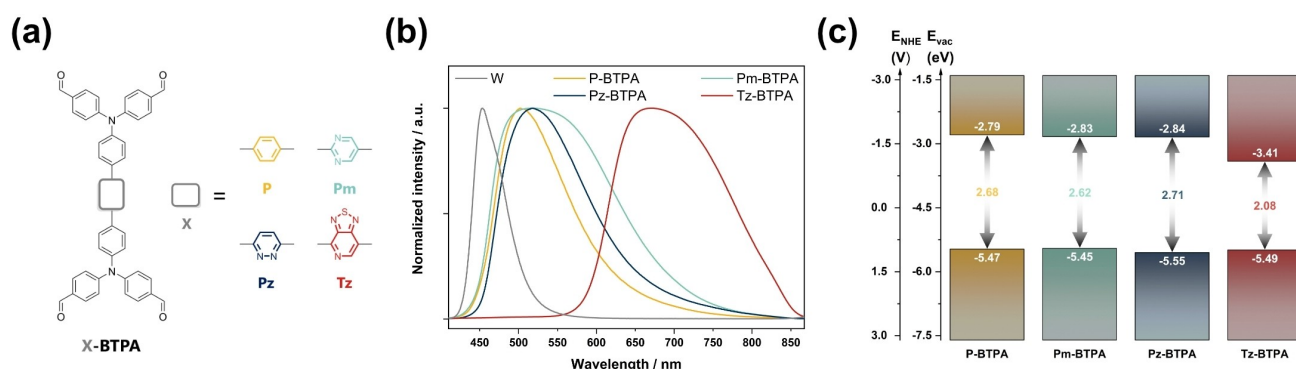


Figure 1. (a) Schematic representation of X-BTPA aldehyde molecules. (b) Normalized PL spectra of the aldehyde X-BTPA and Wurster amine (W) precursor bulk powders. The W amine (grey) exhibits a narrow emission band in the blue spectral range whereas the P- (orange), Pm- (turquoise), Pz- (dark blue) and Tz- (red) BTPA aldehyde precursors show broader PL emission extending towards longer wavelengths. (c) Energy levels of the different aldehyde molecules vs. vacuum and normal hydrogen electrode (NHE).

ing Tz unit shifts the absorption spectrum of the Tz-BTPA up to 650 nm (see Figure S2) as well as the PL emission band by up to 170 nm compared to the P-BTPA with the phenyl (P) unit (Figure 1b). Moreover, this distinct acceptor influence was also reflected in the emitting colors under UV irradiation in chloroform solution, where a light-blue emission and a reddish emission was observed by naked eye for the P- and Tz-BTPA, respectively (see Figure S3).

To compare the PL decay dynamics of the aforementioned chromophore powders, time-correlated single photon counting (TCSPC) was employed using a biexponential fit for the decay curve obtained (Figure S4 and Table S3). Here, the Tz-BTPA exhibits longer lifetimes compared to P-BTPA, attributed to a stabilization of the excited ICT state resulting in longer-lived charge carriers before recombination. The influence of the D-A strength on the band gaps of the building blocks was further investigated by analyzing the highest occupied molecular orbital (HOMO) and lowest unoccupied molecular orbital (LUMO) energy levels from the oxidation and reduction onset potentials detected in cyclic voltammetry (CV) (see Figure 1c and S6).^[25] The HOMO level thereby shifts to smaller eV values, leading to a decrease of the band gap by around 0.6–0.7 eV for the Tz-BTPA compared with its analogs. The band gaps could be confirmed by extracting optical band gaps from Tauc plots (assuming a direct electronic transition) resulting in similar band gap energies for all BTPA-based molecules (Figure S5 and Table S4).

Synthesis of D-A-D COF Systems

Next, the different aldehyde-functionalized building blocks were combined with the Wurster amine (W) under solvothermal conditions. Briefly, the building blocks reacted in a mixture of mesitylene and benzyl alcohol with 6 M acetic acid as catalyst at 120 °C for 72 hours and the resulting precipitate was afterwards isolated by filtration and washing to yield orange to red powders. In this way a series of novel COFs, namely the X-BTPA W COFs, was synthesized (see Figure 2a). Fourier-transform infrared (FT-IR) spectroscopy of the (solid state) precursor and COF powder obtained verified a successful imine-bond formation in the P-BTPA-W COF by showing neither the characteristic C=O stretching vibration of the building block aldehyde groups at 1694 cm⁻¹ nor the N–H vibration of the amine at 3366 cm⁻¹ (see Figure S7). The new absorption band at 1594 cm⁻¹ attributed to the C=N stretching mode^[26] indicates the successful polymerization resulting in the formation of an imine bond.

The powder X-ray diffraction (PXRD) analysis of all COF powders obtained showed high crystallinity and a notable structural similarity due to the close resemblance of the reflection positions and intensities at low angles, constituting the formation of the X-BTPA-W COF series (Figures 2b–f, S8, and Table S5). The Pm-BTPA-W COF and Pz-BTPA-W COF are thereby even constitutional isomeric COFs. To confirm the close structural resemblance, the structures were simulated using the Forcite module of

Materials Studio with the universal force field employing an AA-type, eclipsed layer stacking arrangement giving rise to a dual pore system (Figure S9).^[27] Since the simulated XRD patterns obtained were in good agreement with the experimental data, a Rietveld refinement of the structures with *P1* symmetry was conducted, resulting in low R_p and R_{wp} values (see Figure S10 and Table S6). The reflections apparent in the experimental diffractograms, for instance of the P-BTPA W COF at 2.73, 4.15, 5.00, 5.52, 6.96, 8.36, 10.12 and 20.95° 2θ could be assigned to the *hkl* (010), (100), (110), (020), (120), (030)/(200), (220) and (001) lattice planes, respectively. The 2θ values of the (100), (010) and (001) reflections correspond to lattice plane spacings defining the edge lengths of the unit cell ($a \approx 32$ Å, $b \approx 21$ Å), where the π - π stacking distance (unit cell parameter *c*) can be estimated to be around 4.22 Å for the X-BTPA W COFs, which is 0.2 Å larger than previously reported Wurster-based COFs.^[16] Besides, the COFs exhibited high chemical stability, observed by re-measuring samples using XRD after exposure to various conditions (suspending COF particles in water, sodium hydroxide or hydrochloric acid at room temperature for 2 hours), as well as high thermal stability of up to 400 °C confirmed by thermogravimetric analysis (Figures S11 + S12).

Nitrogen physisorption measurements revealed high Brunauer-Emmett-Teller (BET) surface areas extracted from the isotherm data, with values ranging between 800 and 1000 m² g⁻¹. All adsorption isotherms feature a type-I shape with a steep uptake at low relative partial pressures in agreement with a microporous character (Figure S13). The pore size distributions were calculated using the quenched solid density functional theory (QSDFT) model for 1D cylindrical carbon pores (see insets Figure S13). We note that the distribution maximum for the P-BTPA W COF is split into two peaks resulting in a smaller pore size of 1.46 nm and a larger one of 1.97 nm. A similar split is indicated for the other COFs due to the broadened distribution next to the maximum towards larger pore sizes. These different pore sizes are in good agreement with the simulated orthorhombic pore structures that show two micropores for all X-BTPA W COFs. Using P-BTPA W COF as a representative, its simulated structure resulted in two types of pores with theoretical sizes of 1.42 nm and 2.04 nm (see also Table S7).

The morphology of the bulk materials was further assessed by electron microscopy. Scanning electron microscopy (SEM) images revealed a common general morphology, showing microscopic planar crystallites that intergrow into rosebud-like structures for all COFs (Figure 3a,c, S14). Here, P-BTPA W COF exhibits the largest platelets with sizes of up to 4 μ m in length, while the platelets of the Pz-BTPA W COF are smaller, reaching a size of about 0.5 μ m. In contrast, the small planar particles of the Pm-BTPA W COF tend to intergrow into more compact spherical particles (Figure S14). The high-resolution transmission electron microscopy (TEM) images of P-, Pm- and Tz-BTPA W COF reveal a polycrystalline character and display lattice fringes of highly crystalline elongated particles with sizes of more than 100 nm (Figure 3b,d, S15a,c, S16a).

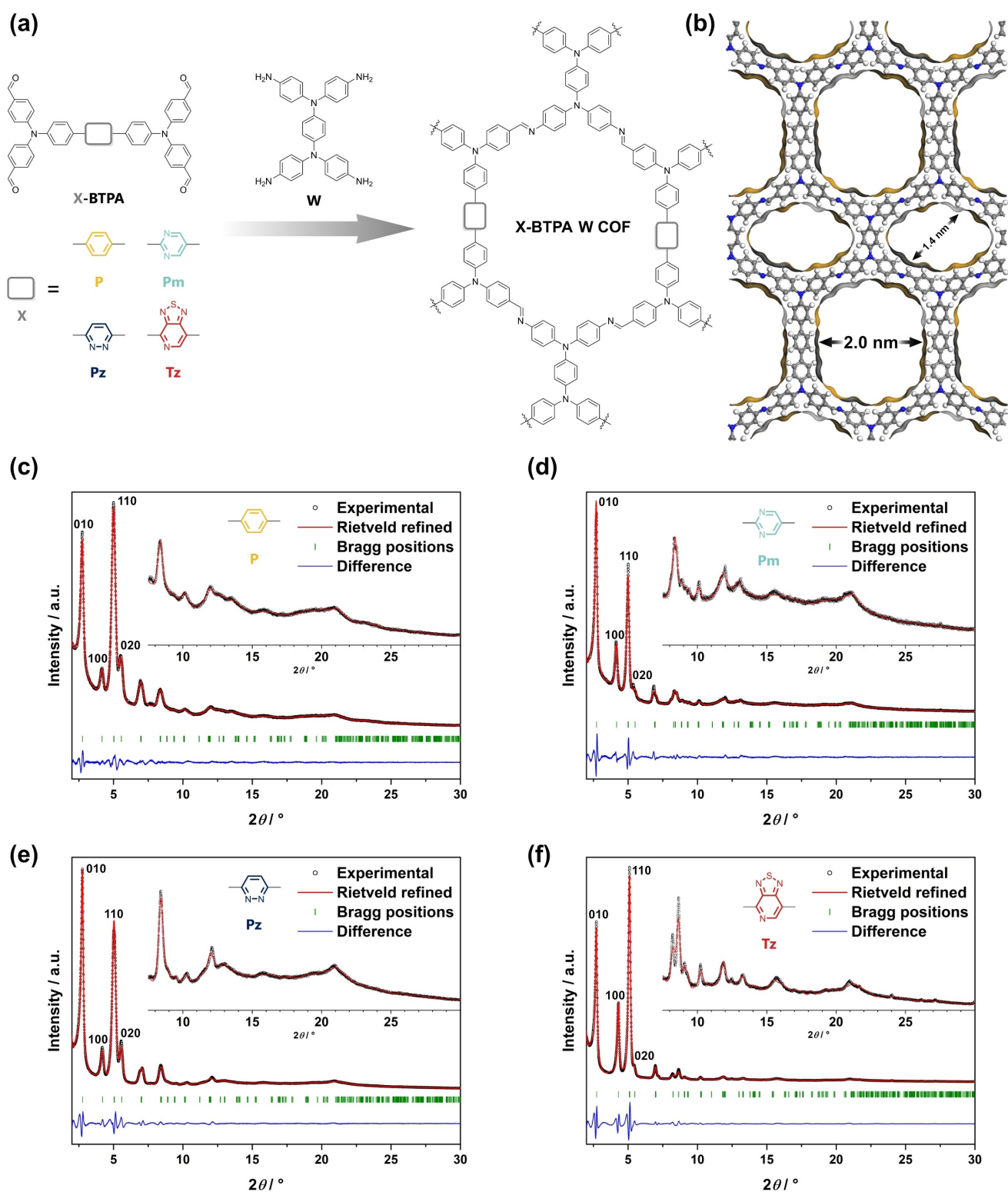


Figure 2. (a) Synthesis scheme of X-BTPA W COF by combining the Wurster amine compound (W) with one of the four different aldehyde-functionalized building blocks P-, Pm-, Pz-, and Tz-BTPA, resulting in 2D COF dual pore topologies, respectively. (b) Simulated structure of P-BTPA W COF monolayer viewed along z-axis. The PXRD patterns (c-f) of each COF reveal high crystallinity, a close resemblance of reflection positions among the different COFs and good agreement between the simulated structures determined by Rietveld refinement. The experimental and Rietveld refined PXRD patterns are of (c) P-, (d) Pm-, (e) Pz- and (f) Tz-BTPA W COF.

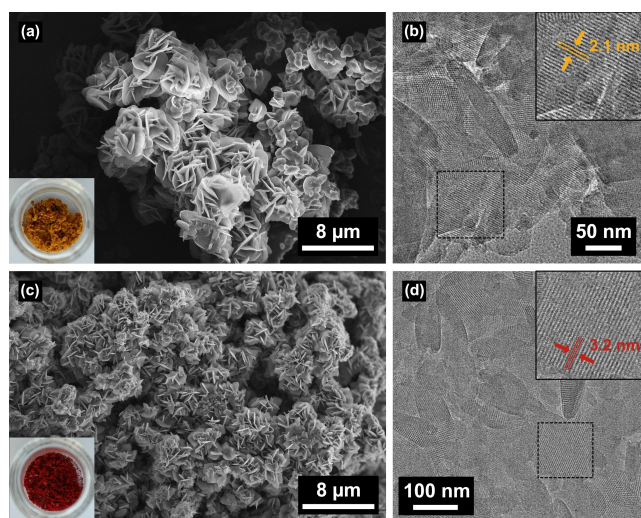


Figure 3. (a,c) SEM and (b,d) TEM images exhibiting the platelet and rosebud-like morphology of P- and Tz-BTPA W COFs, respectively. The inset photographs in (a,c) illustrate the corresponding as-synthesized COF powders, and (b,d) show the marked area enlarged, demonstrating distinct lattice planes of (b) (100) and (d) (010) of the COFs.

Predominant lattice fringes exhibit spacings of 2.1 nm and 3.2 nm that are attributed to the (100) and (010) lattice plane spacings, respectively. Fourier transformation of these images resulted in three circular diffraction lines that can be assigned to the (010), (100) and (110) X-ray diffraction reflections experimentally obtained based on their *d*-spacings (Figure S15b,d, S16b). Besides the minor morphological variations, considerable color differences of the COF powders are observed (Figure 3a, c insets) and in accordance with the variations in the optical absorption spectra (see Figure 4c).

Characterization of Oriented Thin Films

Having successfully established the synthesis of the different D-A Wurster-type COF powders with tunable optical properties, the surface growth of the X-BTPA W COFs was investigated aiming to integrate the COF films as light-absorbing photocathodes in photoelectrochemical water splitting devices. Following the well-established *in-situ* film growth methodology, highly crystalline and oriented COF films were grown by immersing a glass or indium tin oxide (ITO) substrate into a reactive precursor solution under solvothermal reaction conditions following the protocol developed for the COF bulk synthesis.^[28] After 72 h reaction time, uniform COF films at the bottom side of the substrates were observed by naked eye as well as under the optical microscope, showing a yellowish-orange color for the P-, Pm- and Pz-BTPA W COFs and a reddish color for the Tz-BTPA W COF (Figure S17).

Grazing incidence wide-angle X-ray scattering (GI-WAXS) analysis revealed the ordered nature of the resulting films, with reflections at up to $6.3 \text{ nm}^{-1} q_y$ values corresponding to the (200) planes (Figure 4a,b, S19a, S20a,

Table S8). The strong intensities along $q_z = 0 \text{ nm}^{-1}$ confirm a preferential orientation of the films with a parallel layer arrangement of the 2D molecular planes on the substrate and pores perpendicular to the surface, pointing to optimal access of guest molecules and reaction products in and out of the pores. SEM images of substrate cross sections show a homogeneous and fairly uniform coverage with 1.5 to $3.5 \mu\text{m}$ thick plate-like particles protruding from the surface to about $2.5 \mu\text{m}$ (Figure S18–21 b–d). This surface topography provides highly accessible COF surfaces that can be beneficial for photocatalysis applications.^[7] Furthermore, contact angle measurements at the solid/air interface of the COF films with water revealed a hydrophobic behavior of the COF films (Figure S22). By removing a Pz-BTPA W COF film from the substrate, COF domain sizes similar to those of the pure COF powder were revealed by TEM, with identical lattice fringes observed in the Fourier transformation (Figure S16c,d).

To further analyze the tunable light-harvesting properties corresponding to the molecular design of the COF's building blocks, the light absorption profile of all COF films was investigated (Figure 4c). By integrating the strong Tz acceptor unit into the Wurster building block, a significant shift of the UV/Vis spectra with apparent absorption edges from around 500 nm for P-, Pz- and Pm BTPA W COFs to more than 600 nm was induced. Correspondingly, the COF with the P-based building block shows the PL maximum at the shortest wavelength (545 nm) and the Tz-based COF (648 nm) at the longest wavelength (Figure 4d), analogous to the trend observed for the precursor molecules (Figure 1b) and COF bulk material (Figure S24). Furthermore, a red-shift trend of the absorption maxima of the COF series is apparent, where the P- and Tz-BTPA W COF (Table S9) feature a 100 nm difference of the absorption maxima. According to these observations, we attribute the distinct bathochromic shift of the PL bands to the electronic properties of the altered central unit. Hereby, strong electron-withdrawing groups like the Tz moiety shift the PL maximum of the corresponding COF to longer wavelengths by facilitating the photoinduced ICT. Based on the absence of a distinct PL emission band of the (non-altered) Wurster motif itself (at 453 nm for the molecular W amine), we conclude that efficient π -conjugation across the imine bonds has been achieved for the extended framework arrangement of the complete COF.

The ability to specifically tailor the optical properties offers a promising basis for photoelectrochemical applications of the above COFs. We therefore sought to determine the effect of the modified building blocks on the band gap and band positions of the X-BTPA W COFs. Cyclic voltammetry (CV) measurements of the COFs allowed us to estimate the HOMO and LUMO energy levels in a similar manner as for the precursor powders (Figures 4e, S25). Here, no significant changes in the HOMO (between -5.3 eV and -5.2 eV vs. vacuum) were observed when changing the acceptor strength, whereas the LUMO shifted from around -2.9 eV for the P-, Pm- and Pz-BTPA W to -3.3 eV vs. vacuum for the Tz-BTPA W COF. As a result, the electrochemical band gap reduces from around 2.4 eV

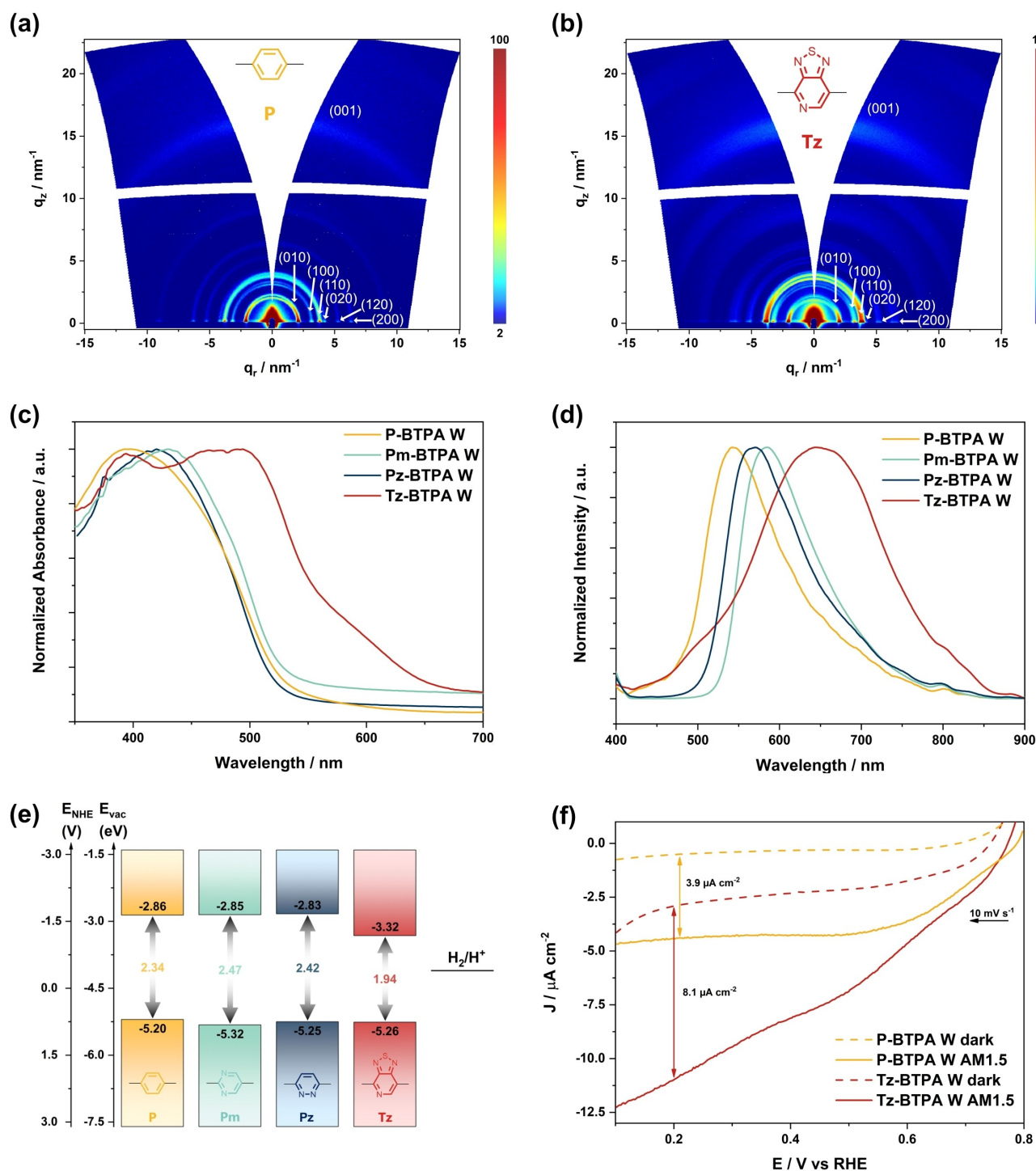


Figure 4. (a,b) GIWAXS two-dimensional patterns of (a) P- and (b) Tz-BTPA W COF films on glass substrates. (c) Normalized absorption and (d) photoluminescence spectra of the oriented COF films. (e) Energy levels of the different COFs vs. vacuum and normal hydrogen electrode (NHE) at pH=0. The energy level of H_2/H^+ was adapted at pH 6.8 given their Nernstian behavior under standard conditions. (f) Linear sweep voltammetry (LSV) of P- (yellow) and Tz-BTPA W (red) photocathode films on ITO performed in the dark (dashed lines) and under AM 1.5 G illumination through the substrate (solid lines).

down to 1.94 eV (in good agreement with the optical band gap) for the P-, Pm- and Pz-BTPA W COFs, while the optical band gap for the Tz-BTPA W COF is slightly larger than the electrochemical one (see Figure S23, Table S9). A potential explanation may be facilitated charge transfer

within the COF layers due to the strong acceptor unit reinforcing the redox process in the framework and therefore shifting the reduction onset towards higher potentials. Because of the redox nature of the building blocks, the band gap detected by electrochemical analysis offers a presumably

more accurate determination of the band gap energies compared to the optical Tauc plot method.^[29]

Photoelectrochemical Water Splitting

The band gaps obtained for the different COF films discussed above, together with the fact that the Pm, Pz and Tz moieties are regularly used as components of photoactive materials in photocatalytic systems, provided the basis for the characterization of the COF films in photoelectrochemical devices. For this purpose, first electrochemical impedance spectroscopy (EIS) measurements were performed revealing relatively low charge-transfer resistances (R_{ct}) ranging between 65 Ω (P-BTPA W) and 1.6 k Ω (Pz-BTPA W) for the COF films. This agrees with the trend observed for the contact angle measurements, namely higher R_{ct} values for more hydrophobic COF films that interact poorly with water (Figure S26, Table S10). Next, linear sweep voltammetry (LSV) was employed in a nitrogen-purged 0.1 M Na₂SO₄ solution under AM 1.5 G illumination through the COF electrode and without illumination in the potential range between 0.8 and 0.1 V vs. reversible hydrogen electrode (RHE) (Figures 4f, S28). Photocurrents starting from around 0.7 V vs. RHE are registered for all X-BTPA W COF films, implying the generation of photoinduced charge carriers. For the P-BTPA W COF, a current density of 3.6 $\mu\text{A cm}^{-2}$ was obtained at 0.55 V_{RHE} and maintained almost constant to 0.1 V_{RHE} . Pm- and Pz-BTPA W COF films exhibit first a reduction feature at around 0.6 V_{RHE} , which is attributed to the redox-active D-A moiety, followed by a similar steady photocurrent development but with higher current densities of up to 4.8 $\mu\text{A cm}^{-2}$ and 6.7 $\mu\text{A cm}^{-2}$ at 0.2 V_{RHE} , respectively. Interestingly, for the case of Tz-BTPA W COF, the current density increased progressively over the whole voltage sweep range, implying the most efficient photogenerated charge transfer of up to 8.1 $\mu\text{A cm}^{-2}$ at 0.2 V_{RHE} , about eight times higher than the highest current density for pure (non-metal-containing) thin and compact COF film photoelectrodes^[6,7] and comparable to other COF materials used as photocathodes for PEC water splitting to date.^[30] Since the high capacitive storage potential of the Wurster motif was previously shown by electrochemical characterization of the W motif,^[16,31] we suggest that the higher dark current observed for the Tz-BTPA W COF may be related to charges present in this enhanced D-A COF. To examine the wavelength-dependence of the photoelectrochemical response, incident-photon-to-current-efficiency (IPCE) of the various COF films was measured (Figure S29). All COFs showed light-to-current conversion activity up to 600 nm with an enhanced range for the D-A-D building blocks, reaching a maximum IPCE of approximately 0.7 % for the Tz-BTPA W COF.

Further, chronoamperometric measurements on COF photoelectrodes were performed at a constant potential of 0.2 V vs. RHE to study the stability of the current density throughout the hydrogen generation. At this potential, the X-BTPA W COF films are stable with a high photoconductivity and a low and stable dark current density. By

illuminating the P- and Tz-BTPA W COF samples at constant intensity over two hours, good stability of the former COF with less than 4 % loss was observed, whereas for the Tz-BTPA W COF film the current density decreased to 60 % of the starting value due to a slight degradation of the COF because of the reduced chemical stability in water (Figure S30). To examine the hydrogen evolution of the X-BTPA W COFs, we employed our previously reported set-up capable of oxidizing the hydrogen generated and dissolved close to the electrode.^[6] Here, a platinum mesh was installed as fourth electrode in front of the active film surface and polarized at 1.1 V vs. RHE. Additionally, illumination and dark intervals were alternated starting from 15-minute and up to 30-minute cycles, while the resulting current density was measured over 6 hours for each sample combined with the oxidation current of the Pt electrode (Figure S31). P-, Pm- and Tz-BTPA W showed consistent photoactive intervals, with a slight decrease in current density and therefore in hydrogen generation over time for the corresponding photocurrent response curves. In contrast, the Pz-BTPA W COF film detached quickly in this measurement configuration, possibly due to weaker attachment of the COF particles to the substrate surface resulting from the preparation process. Furthermore, for the P-BTPA W COF a separation of the film from the surface is observable after two hours, while the crystallinity of all the COFs is maintained after six hours of hydrogen production, with only a slight loss of long-range order revealed by GIWAXS analysis (Figure S32). Moreover, SEM images of the films revealed a persistent morphology with no visible removal of the platelets from the surface (Figure S33). The hydrogen oxidation currents detected at the Pt electrode for P-, Pm-, and Tz-BTPA W COFs surpass the previously reported values of the BDT-ETTA COF^[6] by more than 1 μA and follow the current density trends of the respective COF electrodes, proving the successful hydrogen generation for the thin film COF materials.

Conclusion

Summarizing, this study presents a methodology for tailoring highly crystalline, photoelectrochemically active COFs by condensing isometric D-A-D dyes based on triphenylamine moieties and diverse acceptor units with complementary COF building blocks. This way, the COF's optical properties could be tuned by changing the strength of the acceptor unit. The electronic character of the resulting COFs leads to efficient light absorption and emission in the visible range and enhanced photoinduced intramolecular charge transfer, particularly by the strong electron-withdrawing Tz unit. Based upon their isometric building blocks, the modified Wurster-type COFs created this way displayed close structural and morphological similarities in powder as well as oriented film form. The HOMO and LUMO energy levels of the X-BTPA W COFs revealed a trend similar to that of the precursor molecules, with a significantly reduced band gap for the COF embedding the Tz-acceptor moiety. By increasing the acceptor strength, a more than doubled

current density for photoelectrochemical water splitting at 0.2 V vs. RHE compared to the COF bearing the phenyl core unit could be achieved. This study motivates the development of novel series of D-A COFs with tunable optoelectronic properties by embedding isometric building blocks with different donor/acceptor features in the frameworks.

Supporting Information

The authors have cited additional references within the Supporting Information.^[32]

Acknowledgements

The research leading to these results has received funding from the European Research Council under the European Union's Seventh Framework Programme (FP7/2007-2013/ERC grant agreement 321339). The authors acknowledge funding from the Bavarian Network "Solar Technologies Go Hybrid" and the DFG Excellence Cluster e-conversion (EXC 2089/1-390776260). We acknowledge Dr. Steffen Schmidt for the preparation of the SEM images. The authors thank Dr. Markus Döblinger for electron microscopy. Open Access funding enabled and organized by Projekt DEAL.

Conflict of Interest

The authors declare no conflict of interest.

Data Availability Statement

The data that support the findings of this study are available in the supplementary material of this article.

Keywords: covalent organic frameworks · thin films · donor-acceptor systems · optical properties · photoelectrochemical water splitting

- [1] a) A. P. Côté, A. I. Benin, N. W. Ockwig, M. O'Keeffe, A. J. Matzger, O. M. Yaghi, *Science* **2005**, *310*, 1166; b) N. Keller, T. Bein, *Chem. Soc. Rev.* **2021**, *50*, 1813.
- [2] a) S. S. Han, H. Furukawa, O. M. Yaghi, W. A. Goddard, *J. Am. Chem. Soc.* **2008**, *130*, 11580; b) L. Xia, F. Wang, Q. Liu, *Mater. Lett.* **2016**, *162*, 9; c) C. R. DeBlase, K. E. Silberstein, T.-T. Truong, H. D. Abruña, W. R. Dichtel, *J. Am. Chem. Soc.* **2013**, *135*, 16821; d) F. Xu, H. Xu, X. Chen, D. Wu, Y. Wu, H. Liu, C. Gu, R. Fu, D. Jiang, *Angew. Chem. Int. Ed.* **2015**, *54*, 6814.
- [3] a) D. Bessinger, K. Muggli, M. Beetz, F. Auras, T. Bein, *J. Am. Chem. Soc.* **2021**, *143*, 7351; b) S. Bag, H. S. Sasmal, S. P. Chaudhary, K. Dey, D. Blätte, R. Guntermann, Y. Zhang, M. Položij, A. Kuc, A. Shelke et al., *J. Am. Chem. Soc.* **2023**.
- [4] H. B. Aiyappa, J. Thote, D. B. Shinde, R. Banerjee, S. Kurungot, *Chem. Mater.* **2016**, *28*, 4375.
- [5] a) P. Pachfule, A. Acharjya, J. Roeser, T. Langenhahn, M. Schwarz, R. Schomäcker, A. Thomas, J. Schmidt, *J. Am. Chem. Soc.* **2018**, *140*, 1423; b) T. Banerjee, K. Gottschling, G. Savasci, C. Ochsenfeld, B. V. Lotsch, *ACS Energy Lett.* **2018**, *3*, 400.
- [6] T. Sick, A. G. Hufnagel, J. Kampmann, I. Kondofersky, M. Calik, J. M. Rotter, A. Evans, M. Döblinger, S. Herbert, K. Peters et al., *J. Am. Chem. Soc.* **2018**, *140*, 2085.
- [7] J. M. Rotter, S. Weinberger, J. Kampmann, T. Sick, M. Shalom, T. Bein, D. D. Medina, *Chem. Mater.* **2019**, *31*, 10008.
- [8] L. Yao, A. Rodríguez-Camargo, M. Xia, D. Mücke, R. Guntermann, Y. Liu, L. Grunenberg, A. Jiménez-Solano, S. T. Emmerling, V. Duppel et al., *J. Am. Chem. Soc.* **2022**, *144*, 10291.
- [9] a) J. Yang, S. Ghosh, J. Roeser, A. Acharjya, C. Penschke, Y. Tsutsui, J. Rabeah, T. Wang, S. Y. Djoko Tameu, M.-Y. Ye et al., *Nat. Commun.* **2022**, *13*, 6317; b) S. Li, R. Ma, S. Xu, T. Zheng, G. Fu, Y. Wu, Z. Liao, Y. Kuang, Y. Hou, D. Wang et al., *J. Am. Chem. Soc.* **2022**, *144*, 13953; c) L. D. Tran, K. F. Presley, J. K. Streit, J. Carpena-Núñez, L. K. Beagle, T. A. Grusenmeyer, M. J. Dalton, R. A. Vaia, L. F. Drummy, N. R. Glavin et al., *Chem. Mater.* **2022**, *34*, 529.
- [10] R. Guntermann, L. Frey, A. Biewald, A. Hartschuh, T. Clark, T. Bein, D. D. Medina, *J. Am. Chem. Soc.* **2024**, *146*, 15869.
- [11] a) C. E. Pelkowski, A. Natraj, C. D. Malliakas, D. W. Burke, M. I. Bardot, Z. Wang, H. Li, W. R. Dichtel, *J. Am. Chem. Soc.* **2023**, *145*, 21798; b) A. Kuc, M. A. Springer, K. Batra, R. Juarez-Mosqueda, C. Wöll, T. Heine, *Adv. Funct. Mater.* **2020**, *30*; c) X. Wu, X. Han, Y. Liu, Y. Liu, Y. Cui, *J. Am. Chem. Soc.* **2018**, *140*, 16124.
- [12] a) N. Singh, D. Yadav, S. V. Mulay, J. Y. Kim, N.-J. Park, J.-O. Baeg, *ACS Appl. Mater. Interfaces* **2021**, *13*, 14122; b) E. Jin, K. Geng, S. Fu, M. A. Addicoat, W. Zheng, S. Xie, J.-S. Hu, X. Hou, X. Wu, Q. Jiang et al., *Angew. Chem. Int. Ed.* **2022**, *61*, e202115020.
- [13] a) J.-L. Sheng, H. Dong, X.-B. Meng, H.-L. Tang, Y.-H. Yao, D.-Q. Liu, L.-L. Bai, F.-M. Zhang, J.-Z. Wei, X.-J. Sun, *ChemCatChem* **2019**, *11*, 2313; b) G.-B. Wang, F.-C. Zhu, Q.-Q. Lin, J.-L. Kan, K.-H. Xie, S. Li, Y. Geng, Y.-B. Dong, *Chem. Commun. (Camb.)* **2021**, *57*, 4464.
- [14] D. Schwarz, A. Acharja, A. Ichangi, P. Lyu, M. V. Opanasenko, F. R. Goßler, T. A. F. König, J. Čejka, P. Nachtigall, A. Thomas et al., *Chemistry* **2018**, *24*, 11916.
- [15] a) H. Yu, J. Zhang, X. Yan, C. Wu, X. Zhu, B. Li, T. Li, Q. Guo, J. Gao, M. Hu et al., *J. Mater. Chem. A* **2022**, *10*, 11010; b) C. Lin, X. Liu, B. Yu, C. Han, L. Gong, C. Wang, Y. Gao, Y. Bian, J. Jiang, *ACS Appl. Mater. Interfaces* **2021**, *13*, 27041.
- [16] J. M. Rotter, R. Guntermann, M. Auth, A. Mähringer, A. Sperlich, V. Dyakonov, D. D. Medina, T. Bein, *Chem. Sci.* **2020**, *11*, 12843.
- [17] a) W. Wang, L. Zhang, T. Wang, Z. Zhang, X. Wang, C. Cheng, X. Liu, *J. Energy Chem.* **2023**, *77*, 543; b) M. Liu, S. Liu, C.-X. Cui, Q. Miao, Y. He, X. Li, Q. Xu, G. Zeng, *Angew. Chem. Int. Ed.* **2022**, e202213522.
- [18] C. Krishnaraj, H. Sekhar Jena, L. Bourda, A. Laemont, P. Pachfule, J. Roeser, C. V. Chandran, S. Borgmans, S. M. J. Rogge, K. Leus et al., *J. Am. Chem. Soc.* **2020**, *142*, 20107.
- [19] F. Yu, W. Liu, S.-W. Ke, M. Kurmoo, J.-L. Zuo, Q. Zhang, *Nat. Commun.* **2020**, *11*, 5534.
- [20] T. Ishi-i, K. Ikeda, M. Ogawa, Y. Kusakaki, *RSC Adv.* **2015**, *5*, 89171.
- [21] Z.-J. Yin, S.-Q. Xu, T.-G. Zhan, Q.-Y. Qi, Z.-Q. Wu, X. Zhao, *Chem. Commun. (Camb.)* **2017**, *53*, 7266.
- [22] J.-Y. Zeng, X.-S. Wang, B.-R. Xie, M.-J. Li, X.-Z. Zhang, *Angew. Chem. Int. Ed.* **2020**, *59*, 10087.
- [23] J. Zhao, J. Ren, G. Zhang, Z. Zhao, S. Liu, W. Zhang, L. Chen, *Chemistry* **2021**, *27*, 10781.

- [24] X. Lu, S. Fan, J. Wu, X. Jia, Z.-S. Wang, G. Zhou, *J. Org. Chem.* **2014**, *79*, 6480.
- [25] R. Chen, J.-L. Shi, Y. Ma, G. Lin, X. Lang, C. Wang, *Angew. Chem. Int. Ed.* **2019**, *58*, 6430.
- [26] Y. Hou, X. Zhang, C. Wang, D. Qi, Y. Gu, Z. Wang, J. Jiang, *New J. Chem.* **2017**, *41*, 6145.
- [27] A. K. Rappe, C. J. Casewit, K. S. Colwell, W. A. Goddard III, W. M. Skiff, *J. Am. Chem. Soc.* **1992**, *114*, 10024.
- [28] a) J. W. Colson, A. R. Woll, A. Mukherjee, M. P. Levendorf, E. L. Spitler, V. B. Shield, M. G. Spencer, J. Park, W. R. Dichtel, *Science* **2011**, *332*, 228.; b) L. Frey, J. F. Pöhls, M. Hennemann, A. Mähringer, S. Reuter, T. Clark, R. T. Weitz, D. D. Medina, *Adv. Funct. Mater.* **2022**, *32*, 2205949; c) L. Frey, O. Oliveira, A. Sharma, R. Guntermann, S. P. S. Fernandes, K. M. Cid-Seara, H. Abbay, H. Thornes, J. Rocha, M. Döblinger et al., *Angew. Chem. Int. Ed.* **2023**, *62*, e202302872.
- [29] R. E. Aderne, B. G. A. L. Borges, H. C. Ávila, F. von Kieseritzky, J. Hellberg, M. Koehler, M. Cremona, L. S. Roman, C. M. Araujo, M. L. M. Rocco et al., *Mater Adv* **2022**, *3*, 1791.
- [30] S. Xu, H. Sun, M. Addicoat, B. P. Biswal, F. He, S. Park, S. Paasch, T. Zhang, W. Sheng, E. Brunner et al., *Adv. Mater.* **2021**, *33*, e2006274.
- [31] A. F. M. El-Mahdy, M. G. Mohamed, T. H. Mansoure, H.-H. Yu, T. Chen, S.-W. Kuo, *Chem. Commun.* **2019**, *55*, 14890.
- [32] K. S. W. Sing, *Pure Appl. Chem.* **1985**, *57*, 603.

Manuscript received: April 15, 2024

Accepted manuscript online: August 13, 2024

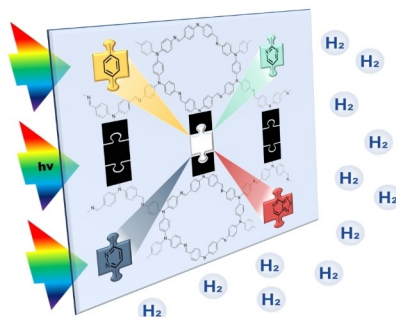
Version of record online: ■■, ■■

Research Article

Photocatalysis

R. Guntermann, D. Helminger, L. Frey,
P. M. Zehetmaier, C. Wangnick, A. Singh,
T. Xue, D. D. Medina,*
T. Bein* _____ e202407166

Tunable Isometric Donor-Acceptor Wurster-
Type Covalent Organic Framework Photo-
cathodes



Covalent organic frameworks (COFs) are crystalline polymeric materials featuring wide-ranging structural control and modularity. The synthesis of a series of donor-acceptor-donor Wurster building blocks enabled the formation of isostructural, photoactive COFs with distinct optical features in thin films. These COFs were further applied for photoelectrochemical water splitting.